HiSST: 3rd International Conference on
High-Speed Vehicle Science Technology
14-19 April 2024, Busan Korea

CEAS
Council of European
Aerospace Societies

Application of HyperCODA to Hypersonic Flows Around Two-Dimensional Geometries

Chiara Amato*, Tobias Ecker†, Tim Horchler‡, Stefan Fechter§, Immo Huismann¶

Abstract

This paper presents a detailed analysis of the HyperCODA flow solver's applicability in studying hypersonic phenomena relevant to both research and industrial contexts. The investigation focuses on exploring HyperCODA capabilities, validating its accuracy, and assessing computational requirements and efficiency in handling high enthalpy flows. Through comparative analysis with the DLR CFD solver TAU, we conducted a detailed study on two specific test cases: a two-dimensional 7/40 degree cone-flare at Mach 5.9 and a free shear layer generated by parallel flows separated by a viscous wall. In particular, the code-to-code comparison is performed between the solutions using an implicit time integration of RANS turbulence modeling, finite volume numerical method, and a single perfect gas. The analysis revealed generally good agreement besides minor discrepancies attributable to the different spatial discretization between the codes. This analysis highlights the potential for further enhancements in HyperCODA, particularly in stabilizing the two-equation turbulent model and addressing variations in flow separation and recirculation areas, thus advancing its utility in hypersonic research and industrial applications.

Keywords: CFD, hypersonic flow, comparative study, RANS, turbulent models

Acronyms

CFD - Computational Fluid Dynamics
CODA – CFD for ONERA, DLR, and Airbus
HEG - High Enthalpy Shock Tunnel in Göttingen
HPC - High-Performance Computing
RANS - Reynolds-averaged Navier-Stokes
SBLI - Shock Boundary Layer Interaction

1 Introduction

In the past decades, the scientific community pushed the limits of space exploration developing ground-breaking designs, such as reusable launchers, hypersonic gliders, and reentry vehicles for interplanetary missions, etc. The substantial growth in complexity of geometries, multi-physics coupling, and chemistry modeling increased the demand for CFD (computational fluid dynamics) software that can support the development of modern hypersonic research. Furthermore, the extraordinary advance of High-Performance computing (HPC) technology has been an essential improvement to be able to handle such demanding problems in terms of grid size, model sophistication and fast develpment cycles. On one side, these codes that target high-enthalpy, high-speed flows, must accurately capture the relevant physico-chemical phenomena characterizing them (shock-induced heating, strong thermochemical non-equilibrium, sharp gradients, etc.). On the other side, they need to be efficient and versatile to make up for lacking of ground testing, to adapt to the variety of configurations, and be structured to run on HPCs.
In the current state-of-the-art at DLR, TAU [1] is a well-established code capable of accurately solving hypersonic flows thanks to the spacecraft extension developed since 2010. However, TAU development started more than two decades ago, and adapting it to the newly available hardware to optimize its performance would require a complete redesign of the code structure.
Hence, since 2018, ONERA, DLR, and Airbus have focused their effort on collectively developing a new generation CFD code called CODA (CFD for ONERA, DLR, and Airbus) based on the structure

*German Aerospace Center, Institute of Aerodynamics and Flow Technology, chiara.amato@dlr.de
†German Aerospace Center, Institute of Aerodynamics and Flow Technology, tobias.ecker@dlr.de
‡German Aerospace Center, Institute of Aerodynamics and Flow Technology, tim.horchler@dlr.de
§German Aerospace Center, Institute of Aerodynamics and Flow Technology, stefan.fechter@dlr.de
¶German Aerospace Center, Institute of Software Methods for Product Virtualization, immo.huismann@dlr.de

and design already employed for the solver Flucs (FLexible Unstructured CFD Software) [2]. This next-generation CFD solver is capable of solving large sparse linear systems derived from the implicit time integration of the RANS (Reynolds-averaged Navier-Stokes) equations with the assumption of a single perfect gas on three-dimensional structured and unstructured grids using either second-order finite-volume or higher-order Discontinuous-Galerkin (DG) discretization.
CODA [3] has been extensively used to solve subsonic and transonic flow regimes because the code has been designed mainly for avionics applications at sub to low supersonic Mach numbers. Thus, as has been done for TAU, DLR has been internally developing an extension for hypersonic applications, HyperCODA [4, 5, 6], that focuses on expanding CODA's physical and numerical modeling capabilities to deal with high enthalpy flows and gas mixtures. This paper aims to explore HyperCODA capabilities and validate its accuracy in solving hypersonic flows around canonical two-dimensional geometries. Making use of the advanced technologies, such as the modern HPC clusters available at DLR, we want to use HyperCODA to solve test cases relevant to the industry and hypersonic research and compare the solutions to DLR CFD solver TAU results and the experimental data from the High Enthalpy Shock Tunnel Göttingen (HEG).
For these reasons, one of the chosen test cases is a 7° cone- 40° flare flying at Mach 5.9. This test case was part of a series of experiments tested at the Calspan-University at Buffalo Research Center (CUBRC) in the Large Energy National Shock (LENS) tunnel, where the scientists considered different angles and inflow conditions. This type of geometry has been extensively studied [7, 8, 9, 10] and used for CFD code validation. The attractions reside in the presence of peculiar physical features in its flow structure, such as Shock Boundary Layer Interaction (SBLI), recirculation region, and separation and reattachment of the flow. Thus, in this paper, we conducted a detailed grid convergence study to ensure a fully resolved flow field and carried out a comparative analysis of the results obtained using HyperCODA and TAU in different regions of interest. Furthermore, the HyperCODA solutions are reported in the Hoste et al. [11] as a part of a blind code-to-code comparison that evaluates the status of RANS modeling for such flows, framing HyperCODA in modern state-of-the-art CFD codes capable of solving complicated hypersonic problems.
The main result highlighted in this comparative analysis is that the HyperCODA results are in almost exact agreement with the TAU results when solving the same turbulence model, as shown in detail in this paper. However, the presented results underpredict the wall heat flux in the zone of interest with respect to the experimental data and the other solutions obtained with the $k-\omega$ turbulence models as a direct and dramatic effect of the chosen turbulent model. We tried to simulate the same problem using the $k-\omega$ turbulence models. However, we encountered difficulties in stabilizing the simulation for this test case. Thus, we decided to investigate the possible reasons behind these difficulties with a simple and canonical test case used in the literature to study turbulence: the compressible shear layer problem. In particular, we replicated the work done by Barone and Oberkampf [12, 13], using this problem also as a validation test for the implementation of the compressible mixing layer correction necessary to stabilize this type of simulations.

2 Test Cases Description

This section contains a detailed description of the test cases chosen for this analysis. In particular, we depict the geometry, collect the initial and boundary conditions, and report the main results of the grid convergence study for both the cone-flare and the shear flow cases.

2.1 7° cone - 40° flare

For this analysis, we are using an axial symmetric grid whose geometrical information is summarized in Figure 1. The grey area in this picture highlights the CFD domain. Its shape was built taking into account the theoretical value of the conical oblique shock wave angle derived using the Taylor-Maccoll function to obtain a grid that is as tailored as possible to the shock. Furthermore, the output region was extended to allow the expected expansion fan to develop around the corner, as well as the interaction between the shock generated at the stagnation point and the second shock wave caused by the flare. The grid details and convergence study are explained in the next sections.

As mentioned in the introduction, this geometry was tested in different setups and inflow conditions in the reflected shock tunnels of the LENS' hypersonic facilities at CUBRC [7, 8, 9, 10]. For this

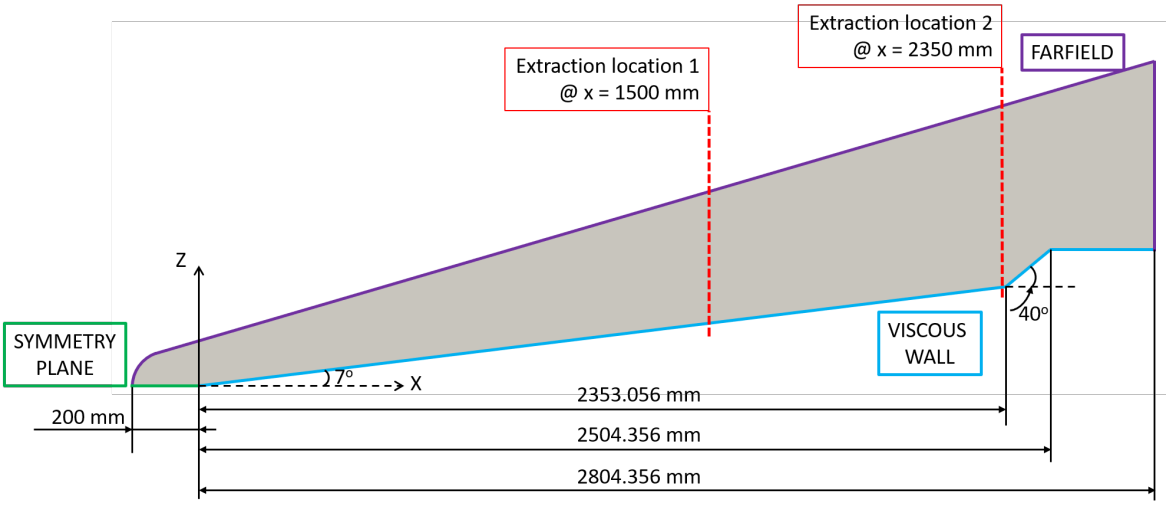

Figure 1: Schematic of the cone-flare CFD domain with the applied boundary conditions

Table 1: Initial and boundary conditions for the 7° cone - 40° flare test case

Free-stream Pressure	7808 Pa
Free-stream Temperature	244.38 K
Free-stream Mach number	5.9
Wall Boundary Condition	Viscous Isothermal Wall
Wall Temperature	300 K
Gas Mixture	Single Perfect Gas with γ=1.4

paper, we chose the inflow conditions corresponding to RUN 45 that are summarized in Table 1. These conditions present a cold wall and non-reactive flow, allowing us to solely focus on the effects of high speed, and the stability of the flows and remove the complexity of including multi-species interactions. The vehicle is flying at Mach 5.9 in a single perfect gas (air, γ=1.4), and the free-stream conditions are equivalent to a flight at around 17.75 km of altitude.

Grid Convergence Study

A detailed grid convergence analysis was conducted focusing on accurately capturing the different scales and physical processes both in the inner portion near the wall, and the outer portion approaching the free stream.

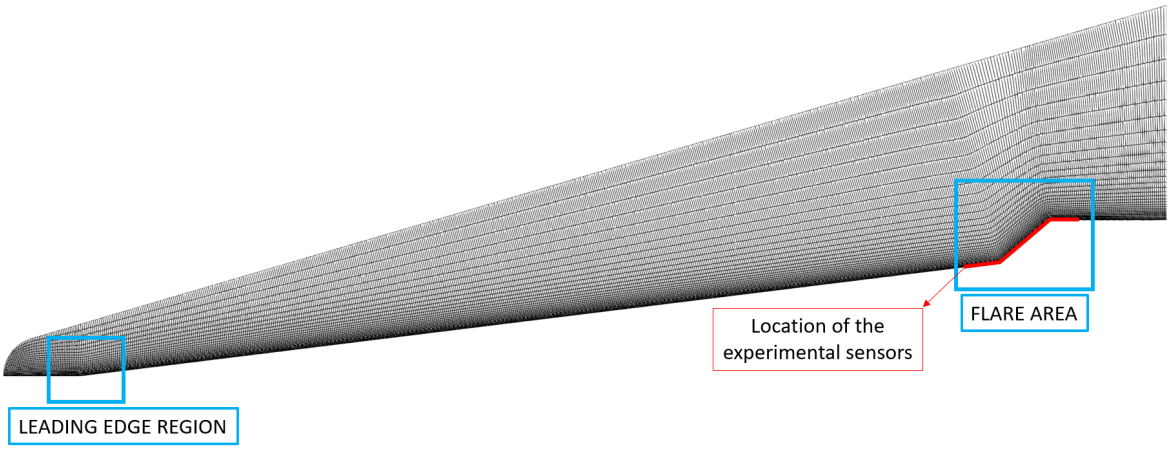

Figure 2: "Very coarse" grid refinement with highlighted regions of interest: leading edge region on the left, and flare area where sensors are located during the experiment at CUBRC [7] on the right

Thus, we built a one-cell wide, one-degree slice of the axisymmetric two-dimensional domain, shown in Figure 1, with an offset of 10^{-8} at the origin. Starting with the most coarse grid shown in Figure 2, we varied the first cell wall spacing δ_{wall}, analyzing three orders of magnitude to guarantee a $y^+<1$ and sufficient resolution for wall heat flux prediction. While expecting a proportional variation of the y^+ with the wall spacing, we can see that $\delta_{wall} = 10^{-4}$ mm is the appropriate trade-off between the ideal value of the y^+ and the computation efficiency due to the minimization of grid points and local time step.

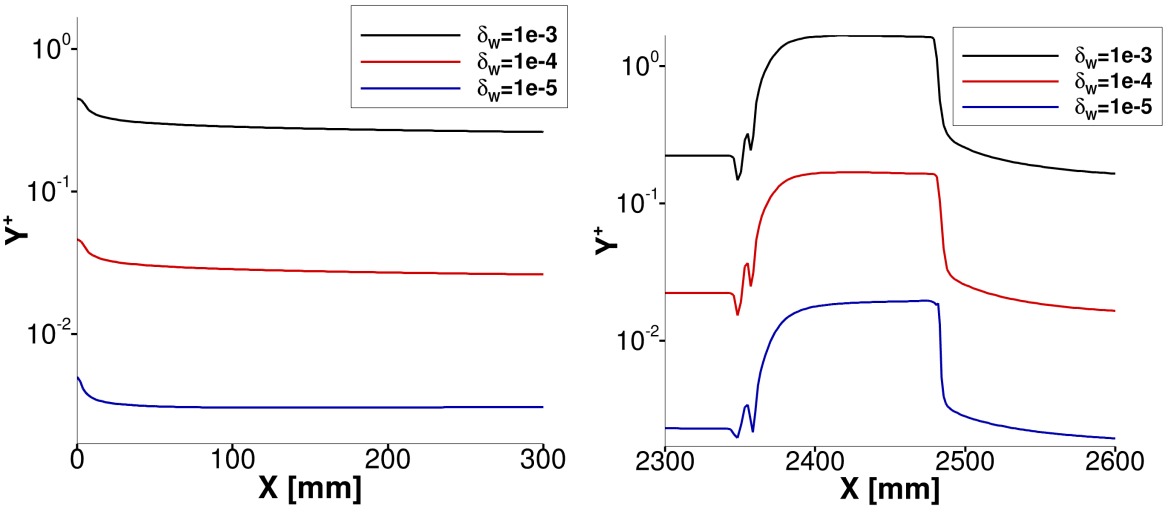

Figure 3: Dimensionless wall distance y^+ distribution on the wall at the leading edge region (left) and the flare area (right) for different first cell wall spacing δ_{wall} (in mm)

Now that the optimal wall spacing has been set, we varied the number of points in both the streamwise and wall-normal directions, doubling up the total number of elements. Table 2 summarizes the different grid resolutions used for this analysis. With the increase of the points in the streamwise direction, we kept clustering the elements around critical areas, such as the stagnation point and the corners. Furthermore, we put extreme carefulness in guaranteeing that the points in these areas are as normal as possible to the wall to avoid grid artifacts and convergence problems (observed in preliminary grids). Table 2 shows the different grid refinement parameters used for this study taken into account for this study with the relative total number of elements.

Table 2: Summary of the mesh refinement considered for the cone-flare simulations

Mesh refinement	Very coarse	Coarse	Medium	Fine	Very fine
Number of elements	60291	121191	243178	586929	793076

First, we decided to use the wall quantities as references for convergence achievement to ensure the regions of interest are well resolved. Hence, as shown in Figure 4a, we are plotting the wall heat flux with respect to the X coordinate in the flare area. It can be seen that the wall heat flux profile of the medium and the fine grids solutions coincide almost exactly, besides a slight difference at location x=2480 mm, where the second corner is located.
Second, we verified that for such resolutions, the outer portion of the flow field approaching the flow field is also fully resolved. Thus, as Figure 4b shows, we extracted the Mach number profile at location x=1500 mm and compared the solutions obtained with the medium, fine, and very fine grids. Although from Figure 4a we can deduce that the medium resolution is sufficient to resolve the wall features, Figure 4b proves that the solution does not reach grid convergence on the medium grid. Thus, we decide to proceed with our analysis with the fine grid since the maximum difference between the solution with the fine and the very fine grid is only Δ_{max}=1.08%.

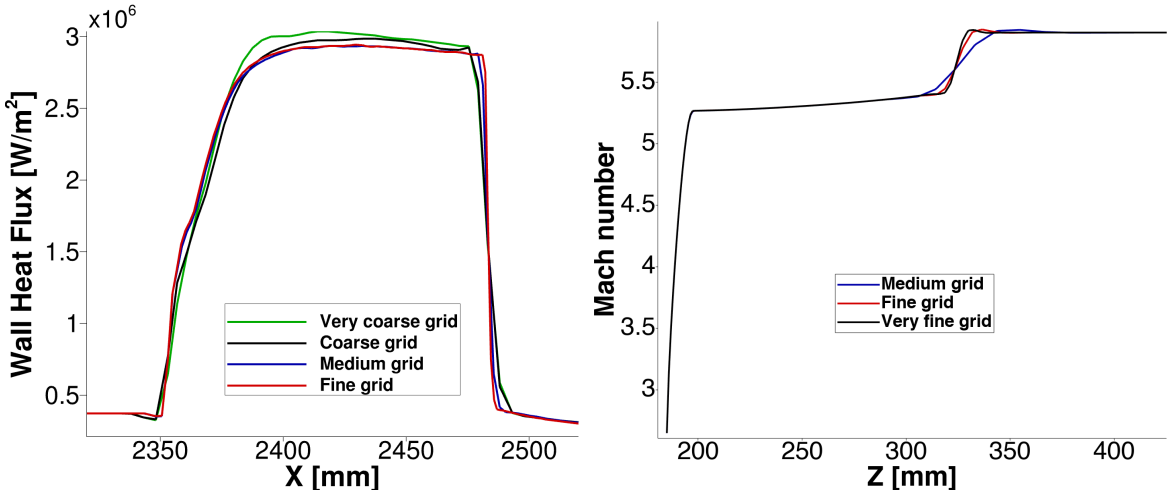

(a) Heat flux profile extracted along the wall for different grid refinements

(b) Mach number profile extracted at x=1500 mm for different grid refinements

Figure 4: Grid convergence study for the cone-flare test case

2.2 Compressible shear layer

The compressible shear layer test case aims to replicate the work done by Barone and Oberkampf in [12, 13]. They set up a problem to study the compressibility effects on the growth rate of a turbulent free-shear layer and develop a new methodology to compare computational results with experimental measurements. In particular, they refer to a canonical turbulent flow configuration where two flows moving at different velocities are initially separated by a very thin wall. Then, the two flows mix downstream of the wall trailing edge, developing into a turbulent free shear layer for high Reynolds numbers.

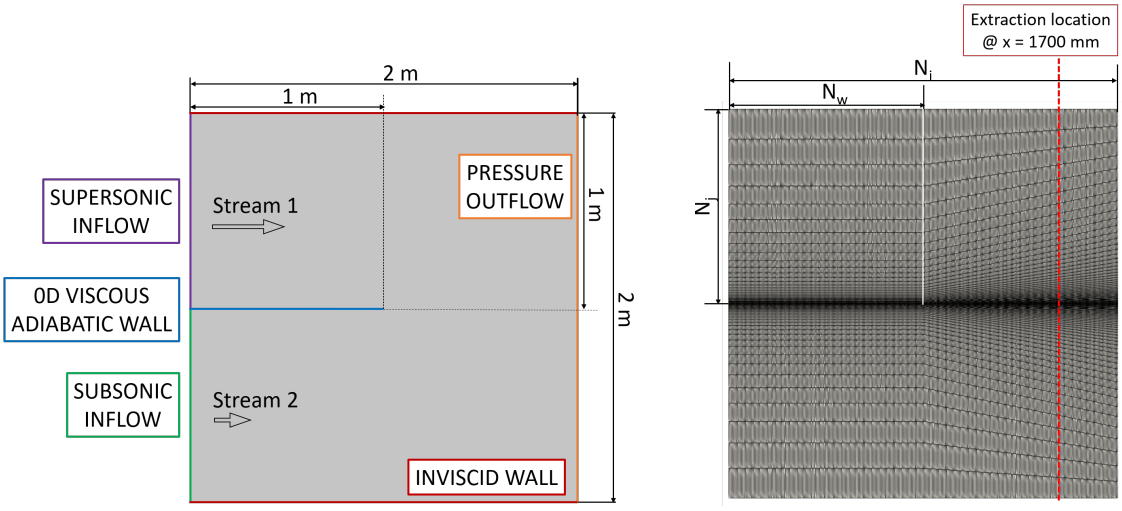

(a) CFD domain and boundary conditions

(b) Coarse grid refinement

Figure 5: Schematics for the shear flow problem

Figure 5a portrays the CFD domain, the geometrical dimension, and the applied boundary conditions used in this study. As it can be seen from Figure 5a, the geometrical size of the domain used in this study is smaller in the wall's normal direction because the flow does not interact with the upper and lower boundary due to the applied farfield boundary condition. Barone et al. [12] proposed a set of eleven test cases where the upper stream Mach number varies from M_1=0.3016 to M_1=6.2347. However, since we are interested in studying HyperCODA performances in hypersonic conditions, we focused on the case with the highest convective Mach number. The inflow conditions related to this case are summarized in Tab. 3.

Table 3: Initial and boundary conditions for the shear flow test case

	Mach number	Free stream density	Free stream pressure	Viscosity ratio	Turbulence intensity
STREAM 1	6.2347	10.1705 [kg/m^3]	100000 [Pa]	1	0.0063246
STREAM 2	0.1	1.16144 [kg/m^3]			

We performed the simulations on the coarse grid, using the number of points reported by Barone et al. [12]. However, since the number of points N_j is distributed over a side half the size, our grid is overall finer than the one proposed by Barone et al. [12]. As it can be seen in Figure 5b, the points are spaced uniformly in the streamwise direction (N_i=300) and clustered around the viscous wall (N_j=68). The viscous wall (N_w=150) is one cell thick, and we set the first cell spacing equal to the thickness of the wall to ensure a unit aspect ratio around the wall. However, since we are expecting the free shear flow to develop downstream of the wall, we increase the spacing in the wall's normal direction in the region between the trailing edge of the wall and the farfield boundary on the left. In this way, the grid is adjusted to the growth of the shear layer thickness.

3 Results: HyperCODA-TAU comparison

In this section, a detailed comparison between the solutions obtained with the flow solvers HyperCODA and TAU is shown for the two chosen test cases.

3.1 Cone-flare test case

One of the aims of this work is to validate the accuracy of HyperCODA in solving high enthalpy flows. Thus, we compare the solutions of the chosen test cases obtained with HyperCODA to the ones obtained using the reference flow solver TAU.

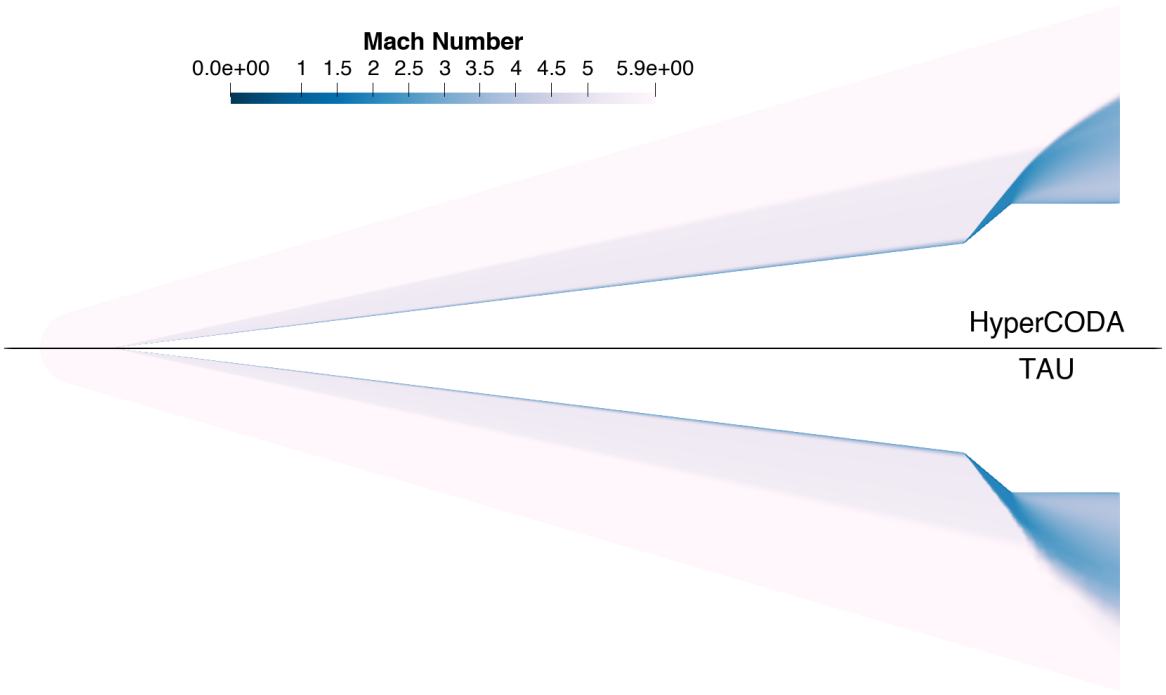

Figure 6: Mach number contour plot comparison of the HyperCODA and the TAU solutions

In HyperCODA, the problem was solved using the two-dimensional structured grid discussed in the previous section. The simulation was run using a second-order finite volume discretization method of

the Reynolds-averaged Navier-Stokes (RANS) equations in combination with the SA-negative turbulence model [14] and the AUSM+M [15] (Advection Upstream Splitting Method) convection scheme. The simulation in TAU was set up consistently in terms of PDE and flux scheme, but it is solving a two-dimensional unstructured grid with around 600K elements. This difference should not affect the quality of the comparison since both grids are the results of a convergence study. Moreover, the two codes use different discretization methods: while HyperCODA is a cell-centered finite volume code, TAU uses a cell vertex with a dual metric spatial discretization.
Figure 6 shows the comparison of the Mach number contour plot of the HyperCODA (on the top) and the TAU (on the bottom) solutions. At first glimpse, we can observe a difference in the outflow area where the two shock waves interact due to the coarseness of the TAU grid in that region. However, this discrepancy is not concerning since we are interested in the comparison up to the flare area included (highlighted in Figure 2), and it does not affect the accuracy of the solution. Thus, we extracted the profiles of the variables of interest at two locations, x=1500 mm and x=2350 mm, as shown in Figure 1.

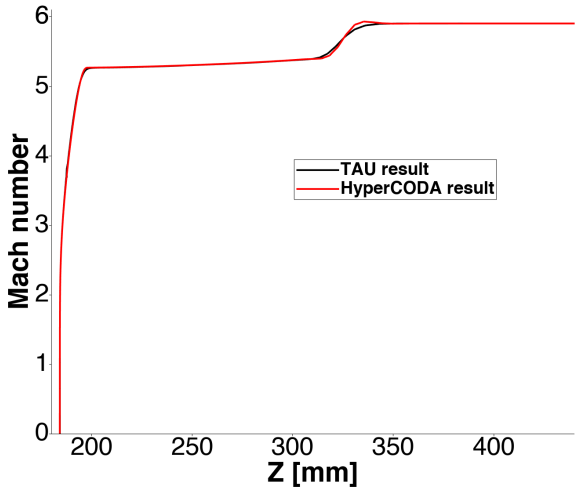

(a) Mach number extracted at x=1500 mm

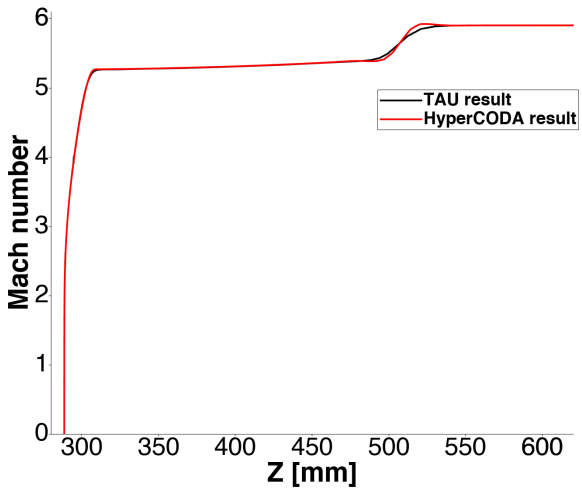

(b) Mach number extracted at x=2350 mm

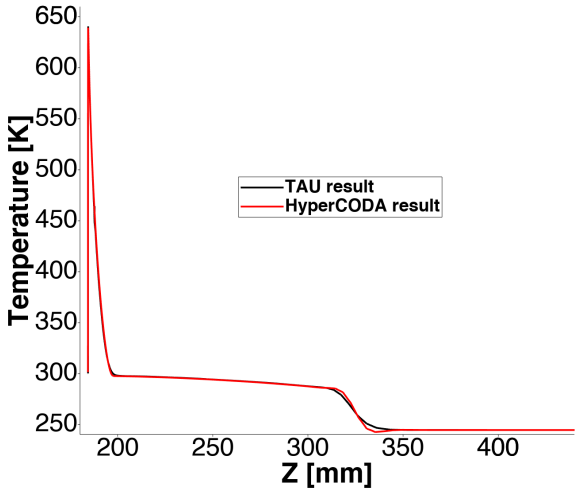

(c) Temperature extracted at x=1500 mm

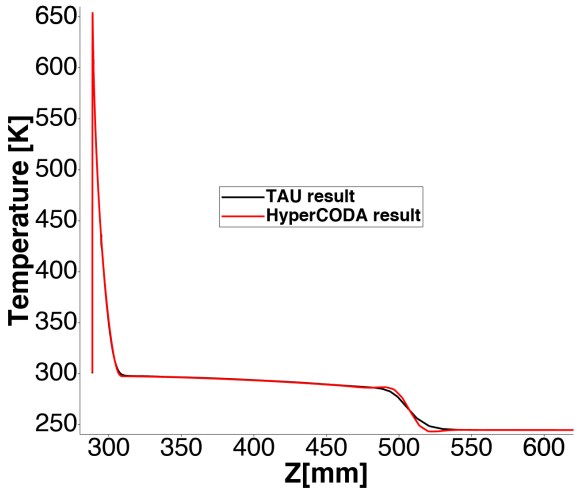

(d) Temperature extracted at x=2350 mm

Figure 7: Comparison of the state variable profiles extracted at two different locations

In Figure 7 the comparison of the state variable profiles can be seen at the two chosen locations, respectively. The black lines are the TAU results, and the red ones are the HyperCODA results. In Figure 7, the comparison shows almost an exact agreement between the solutions. Minor differences are present across the shock wave. In particular, HyperCODA predicts a sharper shock wave than TAU. However, we observe a small overshoot in the Mach number profile, and a small undershoot in the temperature profile for the HyperCODA results. These overshoot/undershoot do not diminish

with further mesh refinement because it was also observed in the solution obtained with the finest mesh. This difference could be due to the presence of a Carbuncle effect stabilizer in TAU that is not present in HyperCODA. This stabilizer may diffuse the solution in the shock region, removing the small overshoot/undershoot present in the HyperCODA solutions. They could also be related to the reconstruction methodology. However, different types of reconstruction have been tested without resolving the problem. Thus, further investigations are needed to fully understand the reasons and address them, if necessary.

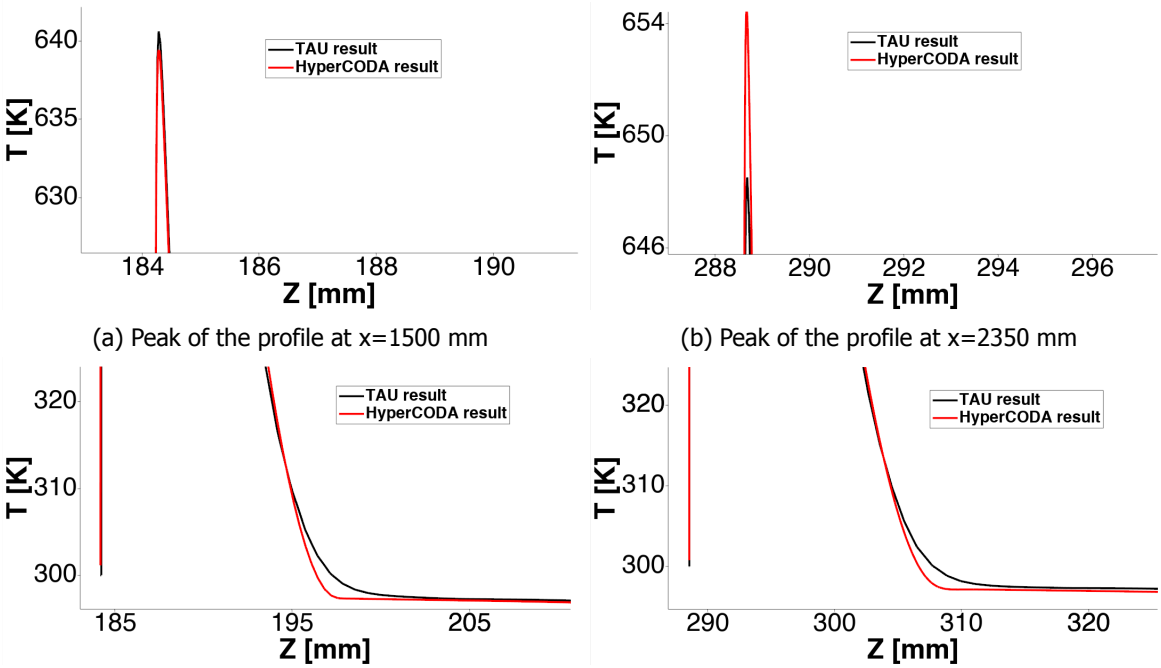

(a) Peak of the profile at x=1500 mm

(b) Peak of the profile at x=2350 mm

(c) Wall region of the profile at x=1500 mm

(d) Wall region of the profile at x=2350 mm

Figure 8: Zoomed plots of the temperature profiles comparison extracted at two different locations

If we zoom around the wall area of Figs. 7c and 7d, we can notice some differences in the prediction of the boundary layer. In particular, Figure 8 collects the zoomed plots of the peak and the wall of the temperature profiles extracted at x=1500 mm, in Figures 8a and 8c, and at x=2350 mm, in Figures 8b and 8d. Altogether, HyperCODA predicted a marginally smaller boundary layer and a sharper edge than the TAU simulation, as shown in Figures 8c and 8d.

Furthermore, Figures 8c and 8d show that TAU foresees a slightly lower temperature at the wall. This disparity is due to the different spatial discretization used by the two codes, and the difference imposition of the boundary conditions. While HyperCODA only imposes the boundary condition in a weak manner via flux computation, TAU sets directly the values at the boundary condition side.

On one side, TAU has the cells centered at the nodes. Thus, the last point is located directly on the wall. For this reason, the extracted profiles show the temperature value imposed by the boundary condition.

On the other side, HyperCODA uses a cell-centered spatial discretization, where the values are stored. Hence, the last points visualized in Figures 8c and 8d reside exactly at a distance equal to half the size of the first cell, showing consequently a slightly higher temperature than TAU. For this reason, we also observe a slightly higher temperature in the peak of the TAU solution shown in Figure 8a. Finally, in Figure 8b, the HyperCODA solution presents a higher peak in temperature than the TAU solution. This behavior can be justified by looking at the separation region located right at the extraction location. In particular, as shown in Figure 9, we can notice that HyperCODA predicts a smaller recirculation bubble than TAU, causing a consequential higher temperature in the boundary layer.

As mentioned in the introduction, these results were added as a part of a global literature review published by Hoste et al. [11]. In that work, the authors performed a blind comparison of the CFD codes available in the hypersonic state-of-the-art. They focused the analysis on comparing wall

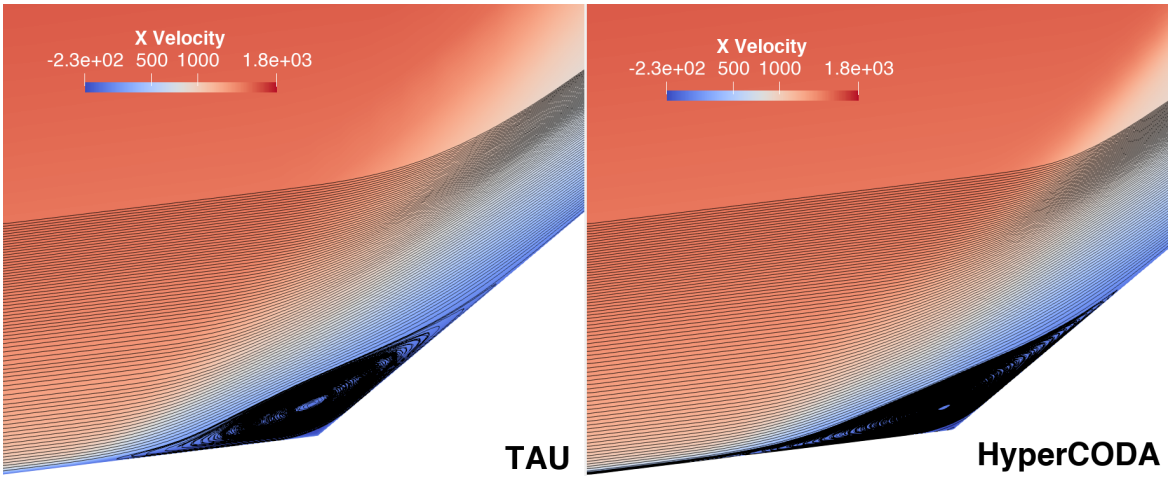

Figure 9: Separation comparison: velocity streamlines superimposed to the x velocity contour plot

pressure and heat flux in the cone-flare area, highlighted in Fig. 2, and characterizing the differences across the chosen turbulence modeling and solvers. The pertinent results and the main points highlighted by this review are summarized hereafter for completion. See Ref. [11] for the details. First, the heat flux profiles predicted with the $k-\omega$ turbulence models align with the experimental data. However, all the solutions predict larger separation bubbles, and therefore, the heat flux peak is located further downstream on the flare geometry with respect to the Schlieren. Second, the HyperCODA and TAU solutions with the SA-negative turbulence model present a lower wall heat flux in the area of interest when compared to other results obtained with the $k-\omega$ turbulence models. These features are to be expected based on the knowledge acquired from previous studies [9]. The authors confirmed that RANS-SAneg turbulence models tend to predict smaller separated regions and a consequential lower wall heat flux. However, the almost exact agreement between HyperCODA and TAU with consistent modeling in Figures 10a and 10b proves that the discrepancies are connected directly to the chosen turbulent model. Furthermore, these trend discrepancies raised the need for additional investigations on HyperCODA capabilities in solving hypersonic turbulent test cases concentrating on the stability of the two-equation models. Hence, the choice to solve the following test cases created the perfect validation case to explore the possible sources of instability and implement well-known corrections for this set of two-equation turbulence models.

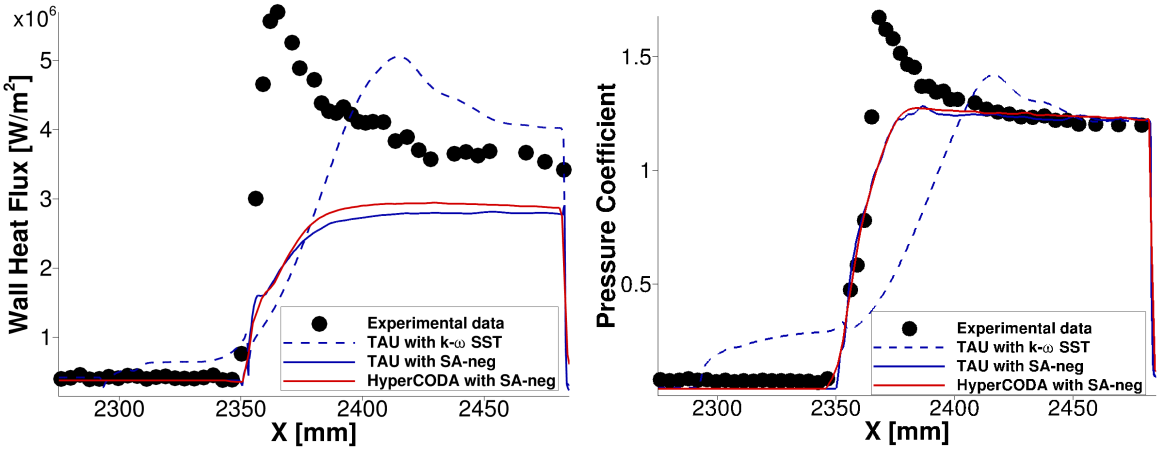

(a) Heat wall profiles

(b) Pressure coefficient profiles

Figure 10: Comparison of the profile in the flare region from the work of Hoste et al. [11]

3.2 Compressible shear layer test case

As already mentioned in the introduction, we selected a canonical test case, such as the compressible shear layer problem, to investigate the state of the art of the two-equation model in HyperCODA. Furthermore, we set it up as a validation case for the compressible mixing layer correction implementation, derived by Wilcox [16, 17]. Thus, we ran the geometry and the inflow conditions described in Section 2.2, using the shear stress transport (SST) formulation of the $k-\omega$ turbulence model developed by Menter [18] with the standard generalized Roe upwinding convection scheme with the low Mach number preconditioning. Moreover, we repeated the simulation with and without the shear layer correction and compared them with the TAU solutions obtained using the same grid and governing equations.
We extracted the state variable profiles at x=1700 mm, shown in Figure 5b, far enough from the trailing edge and not too close to the outflow boundary condition. In this way, the shear layer is fully developed, and the extracted profiles are not affected by the vicinity of the boundary condition. Figure 11 portrays the comparison between the HyperCODA solutions (red lines) and the TAU solutions (black lines). The subsonic region, shown in Fig. 5a, is located in the range $z = [-1000, 0]$, and the supersonic region is from $z = [0, 1000]$. The solid lines are the results obtained with the compressible mixing layer correction, and the dashed lines are the ones without the correction.

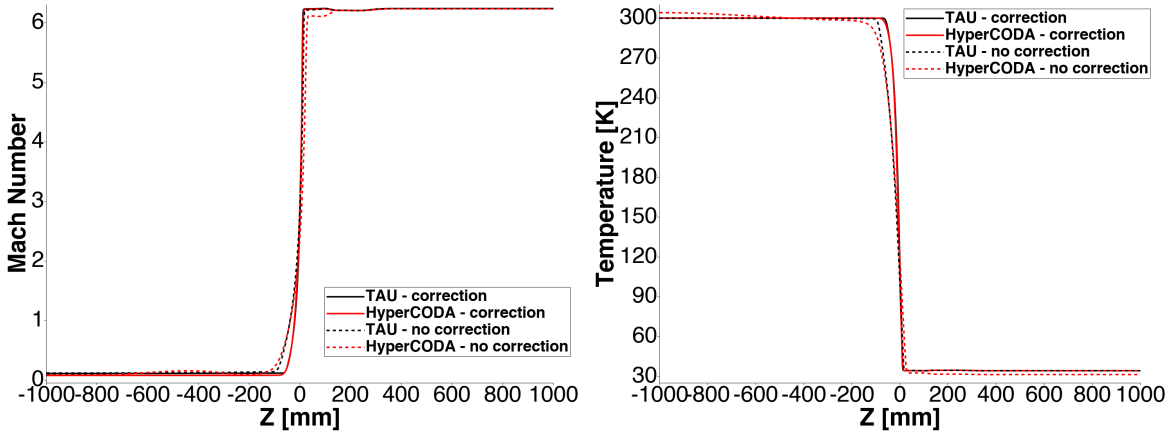

(a) Mach number profile

(b) Temperature profile

Figure 11: State variable profiles comparison of the HyperCODA and TAU solutions, extracted at x=1700 mm, with and without the mixing layer correction

It can be seen that the HyperCODA and TAU solutions are in exact agreement when the mixing layer correction is turned on. However, the profiles extracted from the HyperCODA solution without the correction present some peculiar behaviors not observed in TAU predictions. In particular, from the temperature profile, we can see that the regions far from the shear layer present a higher and lower value, respectively within the subsonic and supersonic flow regions. This behavior can be justified if we analyze the velocity streamlines in the entire domain. In particular, when the correction is not turned on, we can see that the flow is recirculating below the shear layer. A direct consequence is that the overall temperature is slightly higher on that side of the flow and lower where the flow is pulled downstream.
This behavior disappears when the mixing layer correction is turned on because the shear layer thickness is contained. Further investigations are needed to understand the reasons behind this trend. As part of future work, we will increase the size of the domain in the wall's normal direction to verify that these unexpected effects are an interaction caused by the boundary conditions.

4 Conclusion

This paper has examined the application of the flow solver HyperCODA, the hypersonic extension of the new generation CFD code CODA developed internally at DLR, for hypersonic research and

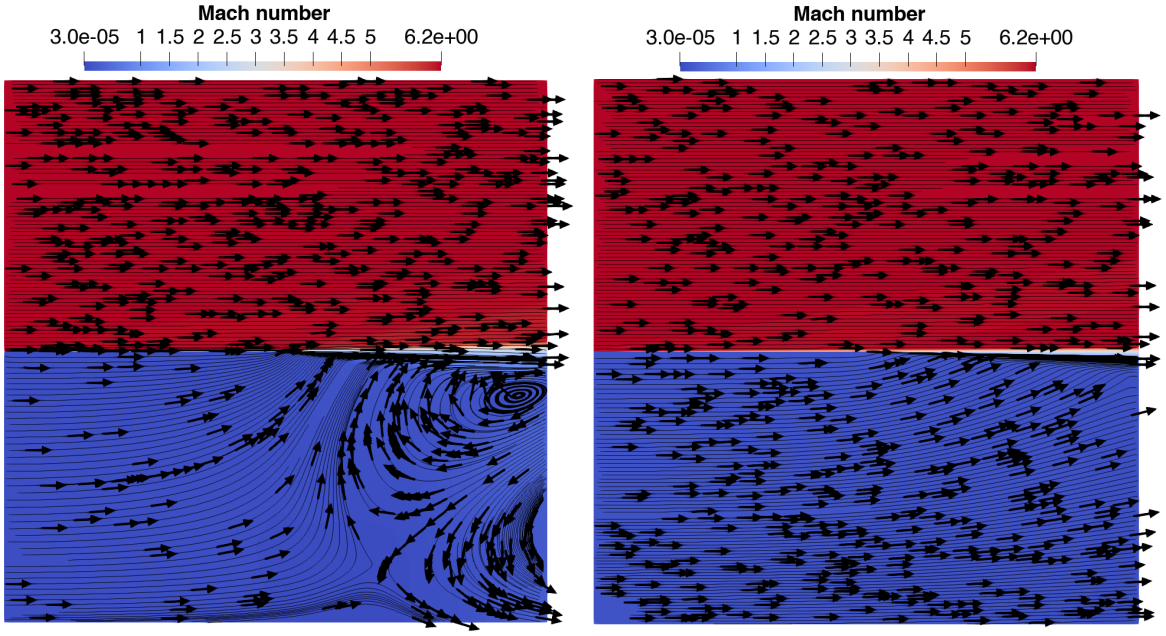

(a) Solution without the compressible mixing layer correction

(b) Solution with the compressible mixing layer correction

Figure 12: Contour plot of the mach number superimposed to the streamlines of the velocity x component for the solution with and without the correction

industrial utilization. Through a detailed analysis, we have delved into HyperCODA's capabilities, computational requirements, and efficacy in solving high-speed flows utilizing two distinct test cases: a two-dimensional $7^\circ/40^\circ$ cone-flare flying at Mach 5.9 and a free shear layer formed by two parallel flows with different velocities initially separated by a viscous wall. To perform this study, we conducted a code-to-code comparison between HyperCODA and the reference DLR CFD solver TAU by setting them as consistent as possible in terms of modeling. In particular, we employed an implicit time integration of RANS turbulence modeling, finite volume numerical method and assumed a single species perfect gas model. The comparative study on the cone-flare was conducted using a structured grid in HyperCODA and an unstructured mesh in TAU. The reasoning behind this choice is because of the underlying difference in the spatial discretization methodologies between the two codes. Regardless of the mesh, it is known and accepted that this difference is reflected in the solutions without affecting the quality of the analysis because it is negligible. Nonetheless, the code-to-code comparison resulted in an almost exact agreement between the solutions obtained by HyperCODA and by TAU.

This comparison was part of a comprehensive literature review published by Hoste et al. [11] on RANS simulations of hypersonic turbulent flow over sharp cone-flares performed by the CFD codes available in the international research community. The HyperCODA and TAU solutions were added to a wide comparison of results obtained with different grids and turbulence models. The HyperCODA results agreed almost exactly when compared with a solution obtained with consistent turbulence modeling, as explained extensively in this paper. Furthermore, HyperCODA pressure is in good agreement with the overall comparison, except in the region where the flow separates. In this same region, HyperCODA underpredicts the wall heat flux with respect to other solutions obtained with the $k-\omega$ turbulence models and the experimental data. This behavior was documented already in studies of Holden and Cross [9], attributing the discrepancies to the chosen turbulent model. On the one hand, it is known that SA turbulence models predict a smaller separated region, an attached flow in the corner, and a lower peak of the wall heat flux. On the other hand, it has been observed that most predictions overestimate the separation bubble since the experimental Schlieren for this run condition does not indicate separation. While the HyperCODA solver remains in its developmental stage, our investigation highlighted the strengths of HyperCODA and underscores the areas for improvement within HyperCODA, particularly stabilizing the two-equation turbulent model and investigating the prediction of recirculation areas. In this regard, preliminary results have been shown in this analysis

with the solution comparison of the second test case, the compressible shear layer. With the intent of minimizing the source of difference between the solutions, HyperCODA and TAU solve the problem by using the same grid and the shear stress transport (SST) formulation of the $k-\omega$ turbulence model. Furthermore, we implemented the compressible shear layer correction proposed in [16, 17] already included in the spacecraft expansion of TAU. The comparison demonstrated an exact agreement in the solutions obtained with the mixing layer correction. Otherwise, the HyperCODA solution shows a recirculation area that does not dissipate in time, not observed in the TAU result. Future work will report on the current work done to address these observations. In particular, an analysis has been conducted showing the sensitivity of the code to the chosen boundary conditions, the reconstruction methods, and the linear solver setting. By addressing these specific areas for improvement, HyperCODA stands poised to offer promising prospects for advancing both research and industrial applications in the field.

References

[1] Langer, S., Schwöppe, A., and Kroll, N., "The DLR Flow Solver TAU - Status and Recent Algorithmic Developments," 2014.

[2] Leicht, T., Jägersküpper, J., Vollmer, D., Schwöppe, A., Hartmann, R., Fiedler, J., and Schlauch, T., "DLR-Project Digital-X-Next Generation CFD Solver'Flucs'," 2016.

[3] Görtz, S., Leicht, T., Couaillier, V., Méheut, M., Larrieu, P., and Champagneux, S., "CODA: A European Perspective for a Next-Generation CFD, Analysis and Design Platform," 2022.

[4] Huismann, I., Fechter, S., and Leicht, T., "HyperCODA–Extension of Flow Solver CODA to Hypersonic Flows," HyperCODA–Extension of Flow Solver CODA Towards Hypersonic Flows, Vol. 13, 2020.

[5] Huismann, I., Fechter, S., and Leicht, T., "HyperCODA–extension of flow solver CODA towards hypersonic flows," New Results in Numerical and Experimental Fluid Mechanics XIII: Contributions to the 22nd STAB/DGLR Symposium, Springer, 2021, pp. 99–109.

[6] Fechter, S. and Huismann, I., "HyperCODA – Extension of Flow Solver CODA Towards Rocket Flows," 2022 9th European Conference for Aerospace Sciences (EUCASS), 2022.

[7] Holden, M., Wadhams, T., MacLean, M., and Mundy, E., "Experimental studies of shock wave/turbulent boundary layer interaction in high Reynolds number supersonic and hypersonic flows to evaluate the performance of CFD codes," 40th fluid dynamics conference and exhibit, 2010, p. 4468.

[8] Holden, M., Wadhams, T., and MacLean, M., "Measurements in Regions of Shock Wave/Turbulent Boundary Layer Interaction from Mach 4 to 10 for Open and "Blind" Code Evaluation/Validation," 21st AIAA Computational Fluid Dynamics Conference, 2013, p. 2836.

[9] Holden, M., Wadhams, T., MacLean, M., and DuFrene, A., "Measurements in regions of shock wave turbulent boundary layer interaction from Mach 3 to Mach 10 for Open and Blind Code Evaluation Validation," Tech. Rep. AFRL-OSR-VA-TR-2013-0134, CUBRC, 2013.

[10] Running, C., Juliano, T., Jewell, J., Borg, M., and Kimmel, R., "Hypersonic shock-wave/boundary-layer interactions on a cone/flare," Experimental Thermal and Fluid Science, Vol. 109, 2019, pp. 109911.

[11] Hoste, J.-J. O., Ecker, T., Amato, C., Gibbons, N., Knight, D., Erin □c Hizir, F., Köktürk, T., Sattarov, A., Thiry, O., Hickey, J.-P., Baurle, R. A., Qiang, S., Coder, J., Castelino, N., and Viti, V., "A code-to-code comparison of turbulent hypersonic sharp cone-flares," HiSST 2024,3rd International Conference on High-Speed Vehicle Science and Technology, 2024.

[12] Barone, M., Oberkampf, W., and Blottner, F., "Validation case study: prediction of compressible turbulent mixing layer growth rate," AIAA journal, Vol. 44, No. 7, 2006, pp. 1488–1497.

[13] Oberkampf, W. L. and Barone, M. F., "Measures of agreement between computation and experiment: validation metrics," Journal of Computational Physics, Vol. 217, No. 1, 2006, pp. 5–36.

[14] Allmaras, S. and Johnson, F., "Modifications and clarifications for the implementation of the Spalart-Allmaras turbulence model," Seventh international conference on computational fluid dynamics (ICCFD7), Vol. 1902, Big Island, HI, 2012.

[15] Chen, S., Cai, F., Xue, H., Wang, N., and Yan, C., "An improved AUSM-family scheme with robustness and accuracy for all Mach number flows," Applied Mathematical Modelling, Vol. 77, 2020, pp. 1065–1081.

[16] Wilcox, D. C., "Dilatation-dissipation corrections for advanced turbulence models," AIAA journal, Vol. 30, No. 11, 1992, pp. 2639–2646.

[17] Wilcox, D. C. et al., Turbulence modeling for CFD, Vol. 2, DCW industries La Canada, CA, 1998.

[18] Menter, F. R., Kuntz, M., Langtry, R., et al., "Ten years of industrial experience with the SST turbulence model," Turbulence, heat and mass transfer, Vol. 4, No. 1, 2003, pp. 625–632.